mathematics

MDPI

Article

Global Dynamics of a Predator–Prey Model with Fear Effect and Impulsive State Feedback Control

Yangyang Su † and **Tongqian Zhang** *,†

College of Mathematics and Systems Science, Shandong University of Science and Technology, Qingdao 266590, China; yangyangsu0320@163.com
* Correspondence: zhangtongqian@sdust.edu.cn
† These authors contributed equally to this work.

Abstract: In this paper, a predator–prey model with fear effect and impulsive state control is proposed and analyzed. By constructing an appropriate Poincaré map, the dynamic properties of the system, including the existence, nonexistence, and stability of periodic solutions are studied. More specifically, based on the biological meaning, the pulse and the phase set are firstly defined in different regions as well as the corresponding Poincaré map. Subsequently, the properties of the Poincaré map are analyzed, and the existence of a periodic solution for the system is investigated according to the properties of the Poincaré map. We found that the existence of the periodic solution for the system completely depends on the property of the Poincaré map. Finally, several examples containing numerical simulations verify the obtained theoretical result.

Keywords: fear effect; impulsive state feedback control; Poincaré map; order-1 periodic solution; stability

MSC: 34C25; 34C60; 37N25; 92D25; 92D45

Citation: Su, Y.; Zhang, T. Global Dynamics of a Predator–Prey Model with Fear Effect and Impulsive State Feedback Control. *Mathematics* **2022**, *10*, 1229. https://doi.org/10.3390/math10081229

Academic Editor: Yonghui Xia and Youhua Qian

Received: 8 February 2022
Accepted: 30 March 2022
Published: 8 April 2022

1. Introduction

As an important branch of ecology, population ecology takes populations as the research object to study the changes and regulation mechanisms affecting population size or quantity in time and space. The complexity of ecological relationships in nature has increasingly required the application of mathematical methods to ecology, which has gradually made mathematical ecology one of the most mature branches of biological mathematics so far. The development of mathematical ecology can be traced back to the study of predator and prey models by the ecologist Lotka [1] and the mathematician Voltra [2] in the first half of the 20th century. Generally, there are four basic types of interactions between the two groups: competing type, mutually beneficial type, parasitic type, predator and prey type. Among them, the predator–prey model has received a great deal of attention and research interest [3–19]. The predator–prey interaction is one of the basic relationships between biological populations, and it is a popular research topic in ecology and biomathematics. A simple model describing the relationship between predator and prey can be written as follows:

$$\begin{cases} \frac{dx}{dt} = x(r_1 - a_{11}x + a_{12}y), \\ \frac{dy}{dt} = y(r_2 - a_{22}y + a_{21}x). \end{cases} \tag{1}$$

However, a new view is that the mere presence of a predator may change the behavior and physiology of the prey such that it can have a more powerful impact on the prey population than in direct predation [20–23]. Animals respond to perceived predation risks and exhibit various anti-predator responses. For example, when the prey is assessing the risk of predation, they may choose to abandon their original high-risk habitats and move to low-risk habitats, which may lead to energy consumption, especially when living conditions in the low-risk habitats are poor [21,24–27]. These changes also include changes in foraging behavior, vigilance, and physiology [21,24–28].

Similarly, fearful prey will reduce their outings for food, and the reduction in food may reduce birth and survival rates. The high risk of acute predation can even cause the prey to temporarily leave the habitat or foraging site [21,22]. Because of the complexity of the interaction between prey and predator, it should not be simply described in terms of direct predation, and the influence of fear should be considered [21,24–27]. As for the extent to which fear affects prey populations, biologists have performed a lot of experiments to show the impact of fear on population size. Recently, Zanette et al. [29] conducted an experiment under the assumption that any impact on reproduction can only be attributed to fear. They broadcast the voice of predators to some songbird populations and found that the fear of predators alone reduced the number of offspring that song sparrows and sparrows could produce by 40%. Biologists attribute this phenomenon to the fear effect, that is, the risk of predation has an impact on the birth rate and survival rate of offspring. It is manifested in the low egg-laying rate of female song sparrows, and the low egg-hatching rate and low survival rate of nestlings. This fear effect has also been found in studies of other species such as other birds [30], elk [31], snow rabbits [32], dugongs [33], and aphids [34,35].

Recently, Wang et al. [36] constructed a predator–prey model with the fear effect, which is written as follows:

$$\begin{cases} \frac{dx}{dt} = r_0 x f(k,y) - dx - ax^2 - g(x)y, \\ \frac{dy}{dt} = y(-d_1 + cg(x)), \end{cases} \tag{2}$$

where r_0 represents the self-growth rate of the prey, d and d_1 are the death rate of preys and predators, respectively. a indicates the mortality rate of the prey due to interspecific competition, $g(x)$ represents the predation function of the predator to the prey, c represents the utilization of energy by predators after ingesting prey, k represents the degree of fear that the bait resists in the face of predation by the predator. It is assumed that the fear effect has an impact on the birth rate of the prey, the term $r_0 x f(k,y)$ involves a factor $f(k,y)$, representing the cost of anti-predator defense due to fear, while the function $f(k,y)$ satisfies the following equation:

$$\begin{cases} f(0,y) = 1, f(k,0) = 1, \lim_{k\to\infty} f(k,y) = 0, \lim_{y\to\infty} f(k,y) = 0, \\ \frac{\partial f(k,y)}{\partial k} < 0, \frac{\partial f(k,y)}{\partial y} < 0. \end{cases}$$

Obviously, the function $f(k,y) = \frac{1}{1+ky}$ meets the conditions above. The authors discussed the dynamics of the model with the functional responses px and $\frac{x}{1+qx}$, respectively. Based on model (2), Zhu et al. [37] proposed a predator–prey model incorporating the fear effect, with the prey and the predator having other food resources:

$$\begin{cases} \frac{dx(t)}{dt} = \frac{r_0 x(t)}{1+ky(t)} - dx(t) - ax^2(t) - bx(t)y(t), \\ \frac{dy(t)}{dt} = cbx(t)y(t) + my(t) - hy^2(t), \end{cases} \tag{3}$$

where m is the utilization of nutrients obtained from other prey for the predator's reproduction, and h is the mortality rate due to environmental density constraints.

State feedback control is the control of the system according to the state of system variables. Because rapid changes in system variables can be described by pulses, it is also called impulsive state feedback control. In the past two decades, impulsive state feedback control has received extensive attention which has been widely used in integrated pest management [38–44], microbial culture [45–51], disease control, and so on [52–60]. Among them, Tang et al. [38] established an impulsive state feedback control system based on a predator–prey system to model the implementation process of integrated pest management:

$$\begin{cases} \left.\begin{array}{l} \frac{dx(t)}{dt} = x(t)(a - by(t)), \\ \frac{dy(t)}{dt} = y(t)(cx(t) - d), \end{array}\right\} x \neq ET, \\ \left.\begin{array}{l} \Delta x(t) = -px(t), \\ \Delta y(t) = \tau, \end{array}\right\} x = ET, \end{cases} \tag{4}$$

where x represents the number of pest populations, y represents the number of natural enemy populations, and ET is the economic threshold, i.e., the number of pests when control measures must be taken to prevent the economic injury level (EIL) from being reached and exceeded, and where the EIL is the lowest pest population density that will cause economic damage. It is assumed that integrated pest management is carried out, and measures such as physical killing, chemical treatment, and biological control are adopted to control the number of the pests when the number of pests reaches the economic threshold (ET).

In this paper, we consider an example of integrated pest management. The bird cherry oat aphid is a small grain aphid common in wheat fields that attacks wheat, oats, rye, and barley. Its common natural enemy is the seven-spotted lady beetle (Coccinella septempuctata). Research has shown that predator odor has an important effect on the growth of the bird cherry oat aphid, and aphids can sense the information left in the surroundings by the seven-spotted lady beetle through hearing, sight, and smell [34]. Moreover, aphids have an innate fear of natural enemies. When the presence of natural enemies is detected, aphids will take further defensive measures [35]. Thus, based on model (3) and model (4), we establish the following system:

$$\begin{cases} \left.\begin{array}{l} \frac{dx(t)}{dt} = \frac{r_0 x(t)}{1+ky(t)} - dx(t) - ax^2(t) - bx(t)y(t), \\ \frac{dy(t)}{dt} = cbx(t)y(t) + my(t) - hy^2(t), \end{array}\right\} x \neq ET, \\ \left.\begin{array}{l} \Delta x(t) = -px(t), \\ \Delta y(t) = -qy(t) + \tau. \end{array}\right\} x = ET, \end{cases} \tag{5}$$

where x represents the number of bird cherry oat aphids, and y represents the number of the seven-spotted lady beetles. $\frac{r_0 x(t)}{1+ky(t)}$ contains the effect of fear of natural enemies. When pest numbers are below ET, we rely on natural enemies in nature to control pest populations. When the pest population reaches ET, integrated pest management will be implemented to suppress the pest population. These include spraying pesticides and releasing predators. That is, the implementation of the control strategy is decided according to the number of pests, which can obviously be represented by a state feedback control system.

Our purpose is to explore the dynamics of the system under impulse state feedback control. The structure of the paper is as follows. Some basic results for model (3) is summarized in Section 2. The dynamics of the system with impulsive state feedback control is discussed using the Poincaré map in Section 3. In Section 4, we give some examples with numerical simulations to verify the obtained theoretical result. In Section 5, we summarize the full paper.

2. Some Basic Results for Model (3)

Without the impulse effect, Zhu et al. studied the dynamic behavior of model (3) (see Theorems 2.1, 2.2, and 3.1 in [37]). Denote $R = \frac{r_0 h^2}{(km+h)(dh+mb)}$; below, we have summarized some basic results in Lemma 1 and Table 1.

Lemma 1. *The system equilibrium point has the following characteristics:*

(a) $E_0(0,0)$ *is always unstable, and it is an unstable node or a saddle point;*
(b) *If* $R > 1$, $E_3(x^*, y^*)$ *is a locally asymptotically stable positive equilibrium, where* $y^* = \frac{m+cbx^*}{h}$ *and* x^* *is the unique positive solution of the equation* $A_1x^2 + A_2x + A_3 = 0$ *where* $A_1 = c^2kb^3 + achkb$, $A_2 = cdhkb + 2ckmb^2 + ahkm + chb^2 + ah^2$, $A_3 = dhkm + km^2 + dh - h^2r_0 + hmb$;
(c) *If* $R < 1$ *and* $r_0 > d$, *the system equilibrium point* $E_1(0, \frac{m}{h})$ *is locally asymptotically stable;*
(d) *If* $r_0 < d$, $E_0(0,0)$ *is a saddle point, point* $E_1(0, \frac{m}{h})$ *is locally asymptotically stable, and point* $E_2(\frac{r_0-d}{a}, 0)$ *does not exist.*

Table 1. Linear analysis of equilibrium points.

Points	$R > 1$	$R < 1$ and $r_0 > d$	$r_0 < d$
$E_0(0,0)$	unstable node	unstable node	saddle
$E_1(0, \frac{m}{h})$	saddle	stable node	stable node
$E_2(\frac{r_0-d}{a}, 0)$	saddle	saddle	does not exist
$E_3(x^*, y^*)$	stable node or focus	does not exist	does not exist

3. Dynamic Analysis of the Model with Impulsive State Feedback Control

3.1. The Impulsive Set and the Phase Set

For system (3), there exist two X-isoclines—$L_1 : x = \frac{r_0}{a(1+ky)} - \frac{d}{a} - \frac{by}{a}$ and the X-axis, and two Y-isoclines—$L_2 : x = \frac{hy}{cb} - \frac{m}{cb}$ and the Y-axis.

Denote the straight lines with $L_3 : x = (1-p)ET$ and $L_4 : x = ET$. The intersection of the straight line L_4 and the isoclinic line L_1 is denoted by $Q(ET, y_{ET})$, where:

$$y_{ET} = \frac{-b - A + \sqrt{(-b+A)^2 + 4kbr_0}}{2kb}, A = kd + kaET.$$

The intersection of the straight line L_3 and the isoclinic line L_1 is denoted by $P((1-p)ET, y_{p_{ET}})$, where:

$$y_{p_{ET}} = \frac{-b - A_1 + \sqrt{(-b+A_1)^2 + 4kbr_0}}{2kb}, A_1 = kd + ka(1-p)ET.$$

The intersection of the straight line L_3 and the isoclinic line L_2 is denoted by $R((1-p)ET, y_{r_{ET}})$, where:

$$y_{r_{ET}} = \frac{cb(1-p)ET + m}{h}.$$

Next, when the system (3) has a stable focus (see Figure 1), we define the impulsive set I_s and the corresponding phase set P_s of the system in two cases.

Case I: $(1-p)ET < ET < x^*$, that is, both the impulsive set and the phase set are on the left of equilibrium E^*. Then, the impulsive set is defined as $I_s = \{(x,y) \in R^2 | x = ET, 0 \le y \le y_{ET}\}$, and the corresponding phase set is defined as $P_s = \{(x^+, y^+) \in R^2 | x^+ = (1-p)ET, y^+ \in D_0\}$, where $D_0 = [\tau, (1-q)y_{ET} + \tau]$ (see Figure 2a).

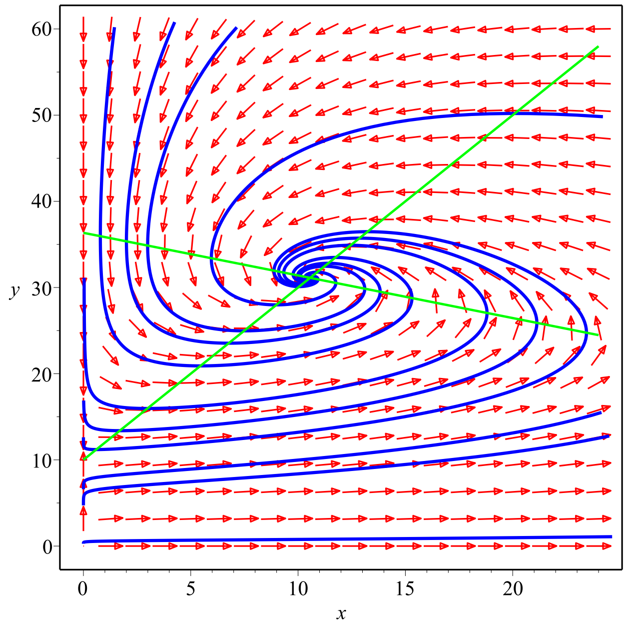

Figure 1. Phase diagram of system (3), with $r_0 = 1.5, k = 0.0003, a = 0.02, d = 0.03, b = 0.04, c = 0.5, m = 0.1, h = 0.01$.

Case II: $(1-p)ET < x^* < ET < \frac{r_0 - d}{a}$, that is, the impulsive set and the phase set are on both sides of equilibrium E^*. Obviously, there is a trajectory Γ and a straight line L_4 tangent to point $Q(ET, y_{ET})$, the intersection of trajectory Γ and isoclines; L_1 is denoted by $P_2(x_{p2}, y_{p2})$. According to the relative position of point $P_2(x_{p2}, y_{p2})$ and straight line L_3, we divide the discussion into two subcases.

Case IIa: If $(1-p)ET < x_{p2}$, the trajectory Γ_1 starting from point $P(ET, y_{p_{ET}})$ will intersect with the line $L_4 : x = ET$ at the point $P_1(ET, y_{p_1})$. At the same time, we found that the point $P((1-p)ET, y_{p_{ET}})$ is the tangent point between the trajectory Γ_1 and the line $L_3 : x = (1-p)ET$. Hence, we have $I_s = \{(x,y) \in R^2 | x = ET, 0 \le y \le y_{p_1}\}$ and $P_s = \{(x^+, y^+) \in R^2 | x^+ = (1-p)ET, y^+ \in D_1\}$, where $D_1 = [\tau, (1-q)y_{p_1} + \tau]$ (see Figure 2b).

Case IIb: If $x_{p_2} < (1-p)ET$, the trajectory Γ and the straight line $L_3 : x = (1-p)ET$ intersect at two points, namely $T_1((1-p)ET, y_{T_1})$ and $T_2((1-q)ET, y_{T_2})$, respectively, where $y_{T_1} < y_{T_2}$. Thus, $I_s = \{(x,y) \in R^2 | x = ET, 0 \le y \le y_{ET}\}$, and we have $P_s = \{(x^+, y^+) \in R^2 | x^+ = (1-p)ET, y^+ \in D_2\}$, where $D_2 = \{[0, y_{T_1}] \cup [y_{T_2}, +\infty)\}$ (see Figure 2c).

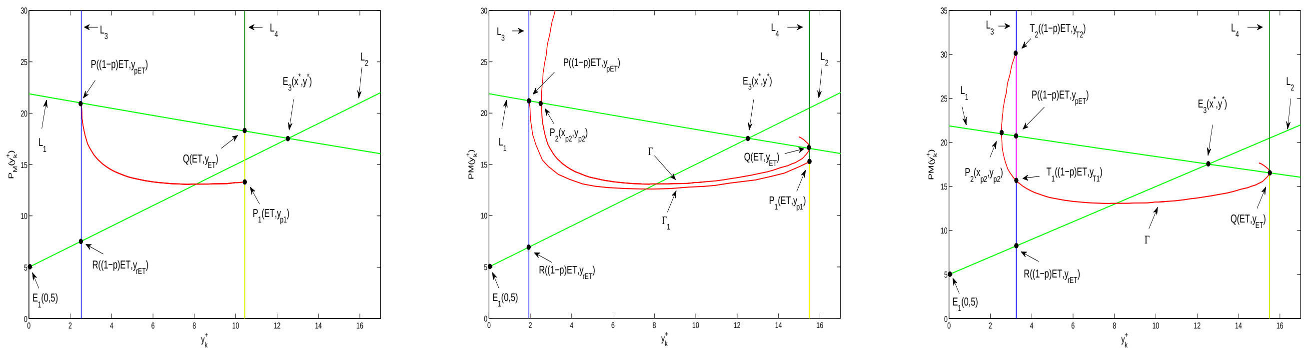

(**a**) (**b**) (**c**)

Figure 2. Impulsive sets and phase sets of different positions. (**a**) $(1-p)ET < ET < x^*$; (**b**) $(1-p)ET < x_{p_2} < x^* < ET$; (**c**) $x_{p_2} < (1-p)ET < x^* < ET$.

3.2. Dynamic Analysis of System (5) for Case I

3.2.1. Definition and Properties of Poincaré Mapping

To establish the Poincaré map of system (5), let us denote two sections as follows: $S_{ET} = \{(x,y)|x = ET, y \geq 0\}$, $S_{p_{ET}} = \{(x,y)|x = (1-p)ET, y \geq 0\}$. We choose section $S_{p_{ET}}$ as the Poincaré section and pick the point $P_k^+ = ((1-p)ET, y_k^+)$ in the Poincaré section $S_{p_{ET}}$. Then, any trajectory $\psi(t, t_0, (1-p)ET, y_k^+) = (x(t, t_0, (1-p)ET, y_k^+), y(t, t_0, (1-p)ET, y_k^+))$ starting from point P_k^+ will intersect with the section S_{ET} at point $P_{k+1} = (ET, y_{k+1})$. Assuming that the elapsed time is t_1, a finite time, then we have $y_{k+1} = y(t_1, t_0, (1-p)ET, y_k^+) = \Phi(y_k^+)$.

For the sake of brevity, let us denote $y((1-p)ET, y_k^+) = y(t_1, t_0, (1-p)ET, y_k^+)$ throughout this paper. When the trajectory $\psi(t, t_0, (1-p)ET, y_k^+)$ of system (5) intersects with the line $x = ET$, $\psi(t, t_0, (1-p)ET, y_k^+)$ will undergo a pulse process and jump to point $P_{k+1}^+ = ((1-p)ET, y_{k+1}^+)$ with $y_{k+1}^+ = (1-q)y_{k+1} + \tau$ on $S_{p_{ET}}$. We need to establish the mapping relationship between P_k^+ and P_{k+1}^+. This is accomplished in two steps. For the first step, let us denote the following:

$$\begin{cases} \frac{r_0 x(t)}{1+ky(t)} - dx(t) - ax^2(t) - bx(t)y(t) = P(x(t), y(t)), \\ cbx(t)y(t) + my(t) - hy^2(t) = Q(x(t), y(t)). \end{cases} \tag{6}$$

Consider the following scalar differential equation in a phase space:

$$\begin{cases} \frac{dy}{dx} = \frac{cbx(t)y(t)+my(t)-hy^2(t)}{\frac{r_0 x(t)}{1+ky(t)} - dx(t) - ax^2(t) - bx(t)y(t)} = g(x,y), \\ y((1-q)ET) = y_0^+. \end{cases} \tag{7}$$

For a given region $\Omega = \{(x,y)|x > 0, y > 0, x < \frac{r_0}{a(1+ky)} - \frac{d}{a} - \frac{by}{a}\}$, obviously, $g(x,y)$ is continuously differentiable on Ω. Let $x_0^+ = (1-p)ET, y_0^+ = S, S \in I_s$, and $S < y_{p_{ET}}$, then $(x_0^+, y_0^+) \in \Omega$. Therefore, we have the following:

$$\begin{aligned} y(x) =& y(x; x_0^+, y_0^+) \\ =& y(x; (1-p)ET, S) \\ =& y(x; S) \\ =& S + \int_{(1-p)ET}^{x} g(s, y(s,S))ds, (1-p)ET \leq x \leq ET. \end{aligned} \tag{8}$$

For the second step, consdering the impulsive effect, we have $y_{k+1}^+ = (1-q)y_{k+1} + \tau$. Therefore, the Poincaré map P_M on Ω can be expressed as follows:

$$P_M(S) = (1-q)y(ET, S) + \tau.$$

The Poincaré map P_M of model (5) satisfies the following properties.

Theorem 1. *The Poincaré map P_M has the following properties:*

(I) *The domain and range of the P_M are $[0, +\infty)$ and $[\tau, (1-q)y((1-p)ET, y_{p_{ET}}) + \tau]$, respectively. They increase on $[0, y_{p_{ET}}]$ and decrease on $(y_{p_{ET}}, +\infty)$;*

(II) *P_M is continuously differentiable;*

(III) *P_M is concave on $[y_{r_{ET}}, y_{p_{ET}}]$;*

(IV) *P_M has a unique positive fixed point y_f. If $\tau > 0$, and $P_M(y_{p_{ET}}) < y_{p_{ET}}$, then $y_f \in (0, y_{p_{ET}})$; if $\tau > 0$, and $P_M(y_{p_{ET}}) > y_{p_{ET}}$, then $y_f \in (y_{p_{ET}}, +\infty)$;*

(V) *For all $y \in [0, +\infty)$, $P_M(y)$ has a maximum value of $P_{M_{max}} = P_M(y_{p_{ET}})$. P_M has a minimum value of $P_{M_{min}} = P_M(0) = \tau$.*

Proof. (I) According to the vector field of system (3), it is easy to see that the definition domain of P_M is $[0, +\infty)$. For any $y_i^+, y_j^+ \in [0, y_{p_{ET}}]$ with $y_i^+ < y_j^+$, by the uniqueness of the solution of model (3), it can be easily obtained that $y((1-p)ET, y_i^+) < y((1-p)ET, y_j^+)$; therefore, we have $P_M(y_i^+) < P_M(y_j^+)$. For any $y_i^+, y_j^+ \in (y_{p_{ET}}, +\infty)$ with $y_i^+ < y_j^+$, according to the the vector field of system (3), the orbit $\phi(t, t_0, (1-p)ET, y_i^+)$ starting from y_i^+ will first intersect with line L_3 and then line L_4, and the intersection with L_3 is denoted by $y_{i'}^+$. The case of the orbits $\phi(t, t_0, (1-p)ET, y_j^+)$ and $\phi(t, t_0, (1-p)ET, y_i^+)$ is similar, and the intersection with L_3 is denoted by $y_{j'}^+$. By the uniqueness of the solution for model (3), we have $y_{i'}^+ > y_{j'}^+$. Then, similarly to the previous case, it can be discussed that $P_M(y_i^+) = P_M(y_{i'}^+) < P_M(y_{j'}^+) = P_M(y_j^+)$. Therefore, P_M is increasing on $[0, y_{p_{ET}}]$ and decreasing on $(y_{p_{ET}}, +\infty)$. Meanwhile, the range of P_M is $[\tau, (1-q)y((1-p)ET, y_{p_{ET}}) + \tau]$.

(II) Since both functions $P(x,y)$ and $Q(x,y)$ are continuous and differentiable, then based on the theorem of Cauchy and Lipschitz along with the parameters we have, P_M is continuous and differentiable.

(III) From (6), we can deduce that:

$$\frac{\partial g}{\partial y} = \frac{cbx + m - 2hy}{\frac{r_0 x}{1+ky} - dx - ax^2 - bxy} + \frac{(bx + \frac{r_0 kx}{(1+ky(t))^2})(cbxy + my - hy^2)}{(\frac{r_0 x}{1+ky} - dx - ax^2 - bxy)^2} \tag{9}$$

and

$$\begin{aligned}\frac{\partial^2 g}{\partial y^2} =& \frac{-2h}{\frac{r_0 x}{1+ky} - dx - ax^2 - bxy} + \frac{(\frac{r_0 kx}{(1+ky)^2} + bx)(cbx + m - 2hy)}{(\frac{r_0 x}{1+ky} - dx - ax^2 - bxy)^2}\\ &+ \frac{-2\frac{r_0 k^2 x}{(1+ky)^3}(cbxy + my - hy^2) + (bx + \frac{r_0 kx}{(1+ky)^2})(cbx + m - 2hy)}{(\frac{r_0 x}{1+ky} - dx - ax^2 - bxy)^2}\\ &+ 2\frac{(\frac{r_0 kx}{(1+ky)^2} + bx)^2(cbxy + my - hy^2)}{(\frac{r_0 x}{1+ky} - dx - ax^2 - bxy)^3}\\ =& \frac{-2h}{\frac{r_0 x}{1+ky} - dx - ax^2 - bxy} + 2\frac{bx(cbx + m - 2hy)}{(\frac{r_0 x}{1+ky} - dx - ax^2 - bxy)^2}\\ &+ 2\frac{\frac{r_0 kx}{(1+ky)^3}(\frac{cbx+m-hy}{1+ky} - hy)}{(\frac{r_0 x}{1+ky} - dx - ax^2 - bxy)^2} + 2\frac{(\frac{r_0 kx}{(1+ky)^2} + bx)^2(cbxy + my - hy^2)}{(\frac{r_0 x}{1+ky} - dx - ax^2 - bxy)^3}.\end{aligned} \tag{10}$$

Since $y_{r_{ET}} < y < y_{p_{ET}}$, we have $\frac{r_0 x}{1+ky} - dx - ax^2 - bxy > 0$ and $cbx + m - hy < 0$, then we obtain $cbx + m - 2hy < 0$. Therefore, we have $\frac{\partial g}{\partial y} < 0$, $\frac{\partial^2 g}{\partial y^2} < 0$ for $y_{r_{ET}} < y < y_{p_{ET}}$. On the other hand, we have the following equation:

$$\begin{aligned}\frac{\partial y(x,S)}{\partial S} =& e^{\int_{(1-p)ET}^{x} \frac{\partial}{\partial y}(\frac{Q(z,y(z,S))}{P(z,y(z,S))})dz} < 0.\\ \frac{\partial^2 y(x,S)}{\partial S^2} =& \frac{\partial y(x,S)}{\partial S}\int_{(1-p)ET}^{x} \frac{\partial^2}{\partial y^2}(\frac{Q(z,y(z,S))}{P(z,y(z,S))})\frac{\partial y(z,S)}{\partial S}dz < 0.\end{aligned} \tag{11}$$

Hence, P_M is monotonically increasing and concave for $y_{r_{ET}} < y < y_{p_{ET}}$.

(IV) Since P_M is decreasing on $(y_{p_{ET}}, +\infty)$, then there exists a $\bar{y} \in (y_{p_{ET}}, +\infty)$ such that $P_M(\bar{y}) < \bar{y}$. In addition, $P_M(0) > 0$ for $\tau > 0$; therefore, there exists $y_f \in [0, \bar{y})$ such that $P_M(y_f) = y_f$, i.e., there exists a fixed point on $[0, +\infty)$ for P_M.

(a) If $\tau > 0$, $P_M(y_{p_{ET}}) < y_{p_{ET}}$, then the fixed point $y_f \in (0, y_{p_{ET}})$. Since P_M is decreasing on $[y_{p_{ET}}, +\infty)$, we have $P_M(y_k^+) < P_M(y_{p_{ET}}) < y_{p_{ET}}$ for $y_k^+ \in [y_{p_{ET}}, +\infty)$, which indicates that no fixed point exists for P_M on $[y_{p_{ET}}, +\infty)$. Next, we prove that the fixed point is unique.

On the one hand, if $P_M(y_{p_{ET}}) < y_{p_{ET}}$ and $P_M(y_{r_{ET}}) > y_{r_{ET}}$, since P_M is concave on $[y_{r_{ET}}, y_{p_{ET}}]$, a unique fixed point thus exists for P_M on $[y_{r_{ET}}, y_{p_{ET}}]$.

On the other hand, if $P_M(y_{p_{ET}}) < y_{p_{ET}}$ and $P_M(y_{r_{ET}}) < y_{r_{ET}}$, there is at least one fixed point on $[0, y_{r_{ET}}]$. If P_M has two fixed points with $\overline{y_1}, \overline{y_2} \in (y_{n1}^+, y_{n2}^+)$, then $P_M(\overline{y_1}) = \overline{y_1}$ and $P_M(\overline{y_2}) = \overline{y_2}$. For any point $y_0^+ \in (y_{n1}^+, \overline{y_1})$, from the successor function, we have $y_0^+ < P_M(y_0^+)$. Since $P_M(\overline{y_1}) = \overline{y_1}$, there is $P_M(y_0^+) < y_0^+$ with $y_0^+ \in (\overline{y_1}, \overline{y_2})$. Similarly, according to $P_M(\overline{y_2}) = \overline{y_2}$ and $P_M(y_{r_{ET}}) < y_{r_{ET}}$, then for any point $y_0^+ \in (\overline{y_2}, y_{n2}^+)$, we have $P_M(y_0^+) < y_0^+$, which contradicts $P_M(y_0^+) < y_0^+$ at any point of $y_0^+ \in (\overline{y_1}, y_{n2}^+)$. Thus, P_M has a unique fixed point y_f on $(0, y_{r_{ET}})$.

(b) If $\tau > 0, P_M(y_{p_{ET}}) > y_{p_{ET}}$, similarly, using the same method in case (a), we can prove that system (5) has only one fixed point in the interval $[y_{p_{ET}}, +\infty)$.

(V) According to the monotonicity of the function P_M and the vector field of system (3), we can easily get that for all $y \in [0, +\infty)$, $P_M(y)$ has a maximum value of $P_{M_{max}} = P_M(y_{p_{ET}})$. P_M has a minimum value of $P_{M_{min}} = P_M(0) = \tau$. □

3.2.2. Existence and Stability of the Boundary Order-1 Periodic Solution for $\tau = 0$

If $y = 0$ and $\tau = 0$, system (5) has a boundary order-1 periodic solution. Then, we discuss the the following subsystem:

$$\begin{cases} \frac{dx(t)}{dt} = (r_0 - d)x(t) - ax^2(t), & x \neq ET, \\ x(t^+) = (1-p)x(t), & x = ET. \end{cases} \tag{12}$$

Take the initial condition $x(0^+) = (1-p)ET$ into (12), then we get the following equation:

$$x(t) = \frac{r_0 - d}{a} \frac{1}{1 + (\frac{r_0 - d}{a(1-p)ET} - 1)e^{-(r_0-d)t}}. \tag{13}$$

Suppose that the trajectory reaches line L_4 at time T, then we obtain the following:

$$ET = \frac{r_0 - d}{a} \frac{1}{1 + (\frac{r_0 - d}{a(1-p)ET} - 1)e^{-(r_0-d)T}}, \tag{14}$$

then, we get the expression of T as follows:

$$T = \frac{1}{r_0 - d} ln \frac{r_0 - d - a(1-p)ET}{(1-p)(r_0 - d - aET)}. \tag{15}$$

Therefore, the periodic solution of $(x^T(t), y^T(t))$ for system (5) is as follows:

$$\begin{cases} x^T(t) = \frac{r_0 - d}{a} \frac{1}{1 + (\frac{r_0 - d}{a(1-p)ET} - 1)e^{-(r_0-d)t}}, \\ y^T(t) = 0. \end{cases} \tag{16}$$

With regard to the stability of the boundary order-1 periodic solution, we have the following theorem.

Theorem 2. *If $\tau = 0$, $\mu_2 < 1$, then the boundary order-1 periodic solution $(x^T(t), 0)$ of system (5) is stable. Furthermore, if $\tau = 0$, $\mu_2 > 1$, the boundary order-1 periodic solution $(x^T(t), 0)$ is unstable.*

Proof. Let us denote the following:

$$\begin{aligned}P(x,y) =&\frac{r_0 x(t)}{1+ky(t)} - dx(t) - ax^2(t) - bx(t)y(t),\\ Q(x,y) =&cbx(t)y(t) + my(t) - hy^2(t),\\ \alpha(x,y) =&-px,\\ \beta(x,y) =&-qy+\tau,\\ \phi(x,y) =&x-ET,\end{aligned} \tag{17}$$

with

$$(x^T(T), y^T(T)) = (ET, 0), (x^T(T^+), y^T(T^+)) = ((1-p)ET, 0).$$

By calculating the partial derivatives with respect to x, y, we get the following equation:

$$\begin{aligned}\frac{\partial P}{\partial x} =&\frac{r_0}{1+ky(t)} - d - 2ax(t) - by(t),\\ \frac{\partial Q}{\partial y} =&cbx(t) + m - 2hy(t),\\ \frac{\partial \alpha}{\partial x} =&-p,\\ \frac{\partial \beta}{\partial y} =&-q,\\ \frac{\partial \phi}{\partial x} =&1,\\ \frac{\partial \alpha}{\partial y} =&\frac{\partial \beta}{\partial x} = \frac{\partial \phi}{\partial y} = 0.\end{aligned} \tag{18}$$

Then,

$$\begin{aligned}\triangle_1 =&\frac{P_+((\frac{\partial\beta}{\partial y})(\frac{\partial\phi}{\partial x}) - (\frac{\partial\beta}{\partial x})(\frac{\partial\phi}{\partial y}) + \frac{\partial\phi}{\partial x}) + Q_+((\frac{\partial\alpha}{\partial x})(\frac{\partial\phi}{\partial y}) - (\frac{\partial\alpha}{\partial y})(\frac{\partial\phi}{\partial x}) + \frac{\partial\phi}{\partial y})}{P(\frac{\partial\phi}{\partial x}) + Q(\frac{\partial\phi}{\partial y})}\\ =&\frac{P_+((x^T(T^+), y^T(T^+)))(1+\frac{\partial\beta}{\partial y})}{P(x^T(T), y^T(T))}\\ =&\frac{(1-p)(1-q)(r_0 - d - a(1-p)ET)}{r_0 - d - aET}.\end{aligned} \tag{19}$$

Let $C = \frac{r_0-d-a(1-p)ET}{a(1-p)ET}$, and we get the equation below:

$$\int_0^T x^T(t)dt =\frac{1}{a}[\ln(e^{(r_0-d)t} + C)]|_0^T. \tag{20}$$

Thus,

$$\begin{aligned}&exp(\int_0^T [\frac{\partial P}{\partial x}(x^T(t), y^T(t)) + \frac{\partial Q}{\partial y}(x^T(t), y^T(t))]dt)\\ &= exp((r_0 + m - d)T + \frac{cb-2a}{a}[\ln(e^{(r_0-d)t} + C)]|_0^T).\end{aligned} \tag{21}$$

Let $\theta = \frac{r_0-d-a(1-p)ET}{(1-p)(r_0-d-aET)}$, thus,

$$
\begin{aligned}
exp(\int_0^T [\frac{\partial P}{\partial x}(x^T(t), y^T(t)) + \frac{\partial Q}{\partial y}(x^T(t), y^T(t))]dt) =& \theta^{\frac{r_0+m-d}{r_0-d}} (\frac{\theta + C}{1+C})^{\frac{cb-2a}{a}} \\
=& \theta^{\frac{r_0+m-d}{r_0-d}} (\frac{r_0 - d - a(1-p)ET}{(r_0 - d - aET)})^{\frac{cb-2a}{a}} \\
=& \theta^{\frac{m}{r_0-d} + \frac{cb}{a} - 1} (1-p)^{\frac{cb}{a} - 2}.
\end{aligned} \tag{22}
$$

Therefore, the Floquet multiplier μ_2 can be calculated as follows:

$$
\begin{aligned}
\mu_2 =& \triangle_1 exp(\int_0^T [\frac{\partial P}{\partial x}(x^T(t), y^T(t)) + \frac{\partial Q}{\partial y}(x^T(t), y^T(t))]dt) \\
=& (1-q)(1-p)^{\frac{cb}{a}} \theta^{\frac{m}{r_0-d} + \frac{cb}{a}},
\end{aligned} \tag{23}
$$

where obviously, if $|\mu_2| < 1$, then the boundary order-1 periodic solution $(x^T(t), 0)$ is stable, and if $|\mu_2| > 1$, the boundary order-1 periodic solution $(x^T(t), 0)$ is unstable. □

Remark 1. *If $q = 0$, from (23), we get the following:*

$$
\mu_2 = (1-p)^{\frac{cb}{a}} \theta^{\frac{m}{r_0-d} + \frac{cb}{a}} = (1-p)^{-\frac{m}{r_0-d}} (\frac{r_0 - d - a(1-p)ET}{r_0 - d - aET})^{\frac{m}{r_0-d} + \frac{cb}{a}}.
$$

Since $R > 1$, then $(1-p)^{-\frac{m}{r_0-d}} > 1$; therefore, $|\mu_2| > 1$ always holds, hence the boundary order-1 periodic solution $(x^T(t), 0)$ of system (5) is always unstable.

3.2.3. Existence and Stability of the Order-1 Periodic Cycle for $\tau > 0$

Theorem 3. *When $\tau > 0$ and $|\mu_2| < 1$, the order-1 periodic solution $(\xi(t), \eta(t))$ is orbitally asymptotically stable.*

Proof. Let T denote the period of the order-1 periodic solution $(\xi(t), \eta(t))$, and the order-1 periodic solution $(\xi(t), \eta(t))$ passes point $M(ET, y_1)$ and point $M^+((1-p)ET, (1-q)y_1 + \tau)$.

Using the calculation method of Theorem 2, we get μ_2,

$$
\begin{aligned}
\mu_2 =& \triangle_1 exp(\int_0^T [\frac{\partial P}{\partial x}(\xi(t), \eta(t)) + \frac{\partial Q}{\partial y}(\xi(t), \eta(t))]dt) \\
=& (1-q)(1-p) \frac{\frac{r_0}{1+k((1-q)y_1+\tau)} - d - a(1-p)ET - b((1-q)y_1 + \tau)}{\frac{r_0}{1+ky_1} - d - aET - by_1} exp(\int_0^T G(t)dt).
\end{aligned} \tag{24}
$$

Therefore, if $|\mu_2| < 1$, the order-1 periodic solution $(\xi(t), \eta(t))$ is orbitally asymptotically stable, and $G(t) = \frac{r_0}{1+k\eta(t)} + (cb - 2a)\xi(t) - (2h + b)\eta(t) + m - d$. □

Theorem 4. *If $P_M(y_{p_{ET}}) < y_{p_{ET}}$, then the Poincaré map P_M has only one stable fixed point y_f on $[0, y_{p_{ET}}]$, and so system (5) has a globally stable order-1 periodic solution.*

Proof. In Theorem 1, P_M is represented as having a single fixed point. Therefore, system (5) has an order-1 periodic solution. In order to narrate the characteristics of the order-1 periodic solution for system (5) more accurately, firstly, the local stability of the fixed point of system (5) is analyzed. From the outcome of Theorem 3, we know that if $\tau > 0$ and $|\mu_2| < 1$, the order-1 periodic solution for system (5) is locally asymptotically stable. Subsequently, the global asymptotic stability of the order-1 periodic solution for system (5) is discussed in the next two intervals: (a) $[0, y_f)$,(b) $[y_f, +\infty)$.

In case (a), any trajectory running from $((1-q)ET, y_0^+)$, $y_0^+ \in [0, y_f)$ will get a series of pulse sequences undergoing multiple pulse processes; the pulse sequence is as follows: $y_0^+ < y_1^+ < y_2^+ < y_3^+ < \cdots < y_n^+ < \cdots < y_f$. In summary, the pulse sequence $P_M^n(y_0^+)$

increases monotonically with the increase of n, and there is $\lim_{n\to\infty} P_M^n(y_0^+) = y_f$. In case (b), for any trajectory from $((1-q)ET, y_0^+)$, $y_0^+ \in [y_f, +\infty)$, after multiple pulses, there are two situations: (i) for all n, $P_M^n(y_0^+) > y_f$ holds; (ii) for all n, $P_M^n(y_0^+) > y_f$ does not hold.

In case (i), the pulse sequence $P_M^n(y_0^+)$ is obtained as follows: $y_f < \cdots < y_n^+ < \cdots < y_3^+ < y_2^+ < y_1^+ < y_0^+$. Therefore, the pulse sequence $P_M^n(y_0^+)$ decreases monotonically with the increase of n. Clearly, there is $\lim_{n\to\infty} P_M^n(y_0^+) = y_f$.

In case (ii), it is surely feasible to find the smallest positive integer n_1 of $P_M^{n_1}(y_0^+) < y_f$. That is, the trajectory with $y_0^+ \in [y_f, +\infty)$ experiences a finite number of pulses, and then intersects with the straight line $x = (1-p)ET$ at point $((1-p)ET, P_M^{n_2}(y_0^+))$, in which $P_M^{n_2}(y_0^+) \in [0, y_f)$.

Therefore, with n_2 increasing, $P_M^{n_2}(y_0^+)$ is monotonically increasing. Eventually, we can get $\lim_{n_2\to\infty} P_M^{n_2}(y_0^+) = y_f$ after going through countless pulses. From the above, it can be seen that the order-1 periodic solution for system (5) is globally asymptotically stable. □

Theorem 5. *If $P_M(y_{p_{ET}}) > y_{p_{ET}}$, then system (5) has an order-1 periodic solution; if $P_M(y_{p_{ET}}) > y_{p_{ET}}$, and any point $y_0^+ \in [y_{p_{ET}}, y_f)$ satisfies $P_M^2(y_0^+) > y_0^+$, then the order-1 periodic solution for system (5) is globally stable.*

Proof. From Theorem 1, we know that if $P_M(y_{p_{ET}}) > y_{p_{ET}}$, then P_M has a unique fixed point y_f. For any $y_0^+ \in [0, y_f)$, there is $P_M(y_0^+) > y_0^+$; for any $y_0^+ \in (y_f, +\infty)$, $P_M(y_0^+) < y_0^+$ holds. According to the convexity of P_M, it can be known that P_M takes the maximum value at point $y_{p_{ET}}$, where $y_{p_{ET}} \in (0, y_f)$.

Firstly, we prove that if all $y_0^+ \in [y_{p_{ET}}, y_f)$ have $P_M^2(y_0^+) > y_0^+$, then the order-1 periodic solution of the system is globally asymptotically stable. Therefore, the global asymptotic stability of the order-1 periodic solution of the system is analyzed in the following three intervals: (a) $y_0^+ \in [y_{p_{ET}}, y_f)$; (b) $y_0^+ \in (0, y_{p_{ET}})$; (c) $y_0^+ \in (y_f, +\infty)$.

For case (a), any trajectory starting from $((1-q)ET, y_0^+)$, $y_0^+ \in [y_{p_{ET}}, y_f)$ has $P_M(y_{p_{ET}}) > P_M(y_0^+) > y_f$ because of the monotonicity of P_M. From Theorem 1, P_M is monotonically increasing on $[y_{p_{ET}}, y_f)$, so P_M^2 is also monotonically increasing on $[y_{p_{ET}}, y_f)$, and $y_0^+ < P_M^2(y_0^+) < y_f$ holds. By induction, we can get $P_M^{2(j-1)}(y_0^+) < P_M^{2j}(y_0^+) < y_f$ (j is a positive integer.) From the pulse sequence, we know that $P_M^{2j}(y_0^+)$ is monotonically increasing, and there are $\lim_{j\longrightarrow+\infty} P_M^{2j}(y_0^+) = y_f$ ($j \geq 1$ and j is a positive integer). In the same way, the monotonicity of $P_M^{2j-1}(y_0^+)$ can be proved.

For case (b), it is known from the pulse sequence that there is a positive integer m that makes $P_M^m(y_0^+) \in [y_{p_{ET}}, y_f)$ or $P_M^m(y_0^+) \in (y_f, +\infty)$ true. If $P_M^m(y_0^+) \in [y_{p_{ET}}, y_f)$, referring to the method in case (a), $P_M^{m+2j}(y_0^+)$ is monotonically increasing, and $\lim_{j\longrightarrow+\infty} P_M^{m+2j}(y_0^+) = y_f$ holds.

If $P_M^m(y_0^+) \in (y_f, +\infty)$, it is known from the pulse relationship that there is $P_M^{m+1}(y_0^+) \in (y_{p_{ET}}, y_f)$, and $\lim_{j\longrightarrow+\infty} P_M^{m+1+2j}(y_0^+) = y_f$.

For case (c), from the discussion method of (b) in Theorem 4, it can be seen that any trajectory starting from point $((1-q)ET, y_0^+)$, $y_0^+ \in (y_f, +\infty)$ will approach a fixed point y_f. In conclusion, if $P_M(y_{p_{ET}}) > y_{p_{ET}}$, and any point $y_0^+ \in [y_{p_{ET}}, y_f)$ satisfies $P_M^2(y_0^+) > y_0^+$, P_M has an order-1 periodic solution which is globally asymptotically stable.

Finally, we prove that if there is a globally asymptotically stable periodic solution, then for any point $y_0^+ \in [y_{p_{ET}}, y_f)$, all holds $P_M^2(y_0^+) > y_0^+$. Conversely, if there is at least one point $\hat{y}^+ \in [y_{p_{ET}}, y_f)$ in $[y_{p_{ET}}, y_f)$, $P_M^2(\hat{y}^+) < \hat{y}^+$ is true. In a small neighborhood of the fixed point y_f, there is a point $\hat{y}^{++}$ in which $P_M^2(\hat{y}^{++}) > \hat{y}^{++}$ holds. Therefore, we know from the successor function that there is another point $y_f^* \in (\hat{y}^+, \hat{y}^{++})$ that makes $P_M^2(y_f^*) = y_f^*$ true. This contradicts the global asymptotic stability of the order-1 periodic solution. Therefore, if there is a globally asymptotically stable periodic solution, it holds $P_M^2(y_0^+) > y_0^+$ for any point $y_0^+ \in [y_{p_{ET}}, y_f)$. □

3.3. Dynamic Analysis of System (5) for Case II

In Case II, we define impulse sets and phase sets in two sub-cases named Case IIa and Case IIb, respectively. Through the analysis of the system trajectories, we find that the definition and properties of the Poincaré map in Case IIa are the same as those in Case I. Then, we can obtain the same properties of the system as in Case I. Here, we do not demonstrate in detail, but we only give relevant conclusions for Case IIa and focus on Case IIb.

Theorem 6. *If $\tau = 0$, $\mu_2 < 1$, then the boundary order-1 periodic solution $(x^T(t), 0)$ for system (5) is stable. Furthermore, if $\tau = 0$, $\mu_2 > 1$, the boundary order-1 periodic solution $(x^T(t), 0)$ is unstable.*

Theorem 7. *When $\tau > 0$ and $|\mu_2| < 1$, the order-1 periodic solution $(\xi(t), \eta(t))$ is orbitally asymptotically stable.*

Theorem 8. *If $P_M(y_{p_{ET}}) < y_{p_{ET}}$, then the Poincaré map P_M only has the globally asymptotically stable fixed point y_f on the interval $[0, y_{p_{ET}}]$, that is, system (5) has an order-1 periodic solution.*

Theorem 9. *If $P_M(y_{p_{ET}}) > y_{p_{ET}}$, system (5) has an order-1 periodic solution; if $P_M(y_{p_{ET}}) > y_{p_{ET}}$ and any point $y_0^+ \in [y_{p_{ET}}, y_f)$ satisfies $P_M^2(y_0^+) > y_0^+$, then the order-1 periodic solution for system (5) is globally stable.*

Next, we analyze the characteristics of Poincaré mapping in case IIb. Different from Case I and Case IIa, the phase set of Case IIb is divided into two disjoint parts (see Figure 2c), such that the Poincaré map of Case IIb has different properties from Case I and Case IIa although their definitions are the same.

3.3.1. Properties of Poincaré Mapping for Case IIb

Theorem 10. *The Poincaré map P_M has the following properties:*

1. *The domain and range of P_M are $D_2 = \{[0, y_{T_1}] \cup [y_{T_2}, +\infty)\}$ and $[\tau, (1-q)y((1-p)ET, y_{T_1}) + \tau]$, respectively. It is increasing on $[0, y_{T_1}]$ and decreasing on $[y_{T_2}, +\infty)$;*
2. *P_M is continuously differentiable on D_2;*
3. *P_M has a unique fixed point y_f or has no fixed point. If $\tau > 0$ and $P_M(y_{T_1}) < y_{T_1}$, then $y_f \in (0, y_{T_1})$; if $\tau > 0$ and $y_{T_1} < P_M(y_{T_1}) < y_{T_2}$, then the system has no fixed point; if $\tau > 0$ and $P_M(y_{T_1}) > y_{T_2}$, then $y_f \in (y_{T_2}, +\infty)$;*
4. *For all $y \in [0, +\infty)$, $P_M(y)$ has maximum value of $P_{M_{max}} = P_M(y_{T_1}) = P_M(y_{T_2})$. P_M has a minimum value of $P_{M_{min}} = P_M(0) = \tau$.*

Proof. The proof is similar to the process in Theorem 1, and here we omit it. □

3.3.2. Existence and Stability of the Order-1 Limit Cycle for Case IIb

From Theorem 10, the Poincaré map has one fixed point or zero fixed points in case IIb. When the Poincaré map has a fixed point, then system (5) has an order-1 periodic solution. In the following, we will discuss the stability of the order-1 periodic solution for the system.

Theorem 11. *For case IIb, if $P_M(y_{T_1}) \le y_{T_1}$ or $P_M(y_{T_1}) \ge y_{T_2}$, then there exists a stable order-1 periodic solution for system (5). If $y_{T_1} < P_M(y_{T_1}) < y_{T_2}$, there is no order-1 periodic solution for system (5).*

Proof. If $P_M(y_{T_1}) = y_{T_1}$ or $P_M(y_{T_1}) = y_{T_2}$, then P_M has a fixed point on $(0, +\infty)$ according to Theorem 10.

If $P_M(y_{T_1}) < y_{T_1}$, then any trajectory initiating from $((1-p)ET, y_0^+)$ experiences impulsive effects n times (infinitely), and we obtain $y_n^+ \in [0, y_{T_1}]$. By Theorem 10, the impulsive point series y_n^+ is monotonically increasing on $[0, y_{T_1}]$ and monotonically decreasing on $[y_{T_2}, +\infty)$. Hence, we have $\lim_{n\to\infty} y_n^+ = y_f$ and $y_f \in [0, y_{T_1}]$. This proves that system (5) has a stable order-1 periodic solution.

If $P_M(y_{T_1}) > y_{T_2}$, then consider two cases: $y_{T_2} < \tau$ and $y_{T_2} > \tau$. When $y_{T_2} < \tau$, then for any trajectory starting from $((1-q)ET, y_0^+)$, $y_0^+ \in D_2$ infinitely passes many pulses, and from the properties of the Poincaré map, there is a unique fixed point on $[y_{T_2}, +\infty)$.

When $y_{T_2} > \tau$, there exists a y_c such that $P_M(y_c) = y_{T_2}$. Moreover, any trajectory initiating from $((1-q)ET, y_0^+)$, $y_0^+ \in [0, y_{T_2}]$ (or $y_0^+ \in [y_c^1, y_c]$ and $0 < y_c^1 < y_c$) will be free from impulsive effects after one single impulsive effect. Thus, system (5) has a stable order-1 periodic solution on $[y_{T_2}, +\infty)$.

If $y_{T_1} < P_M(y_{T_1}) < y_{T_2}$, then any trajectory beginning with $((1-q)ET, y_0^+)$, $y_0^+ \in D_2$ will experience finite pulses and will then leave impulsive effects; finally, they will tend to the open set (y_{T_1}, y_{T_2}). That is, P_M has no order-1 periodic solution. $\square$

By using the same method as Theorem 5, we can prove the following theorem.

Theorem 12. *When $P_M(y_{T_1}) > y_{T_2}$ and any point $y_0^+ \in [y_{T_2}, y_f)$ satisfies $P_M^2(y_0^+) > y_0^+$, then the order-1 periodic solution of system (5) is globally stable.*

4. Numerical Simulation

In this section, we employ some numerical simulations to verify the main results. The basic parameters are chosen as

$$r_0 = 1.5, k = 0.03, a = 0.02, d = 0.03, b = 0.04, c = 0.5, m = 0.1, h = 0.01.$$

Then, we get the following system:

$$\begin{cases} \frac{dx(t)}{dt} = \frac{1.5x(t)}{1+0.03y(t)} - 0.03x(t) - 0.02x^2(t) - 0.04x(t)y(t), \\ \frac{dy(t)}{dt} = 0.02x(t)y(t) + 0.1y(t) - 0.01y^2(t). \end{cases} \tag{25}$$

Through calculation, we get $R = 2.6834 > 1$, then there exist four equilibria, i.e., $E_0 = (0,0)$, $E_1 = (0,10)$, $E_2(\frac{r_0-d}{a}, 0) = (73.5, 0)$, and $E_3(x^*, y^*) = (4.996, 20.139)$. By Theorems 2.1, 2.2, and 3.1 in Zhu et al. [37], we conclude that E_0 is an unstable node, E_1 and E_2 is an unstable saddle point, $E_3(x^*, y^*) = (4.996, 20.139)$ is a stable focus.

Next, we will discuss the dynamics of the system under the effect of the state-dependent impulse control through the following cases.

For the Case I, we will firstly verify the existence and stability of the boundary order-1 periodic solution $(x^T(t), 0)$. Let $p = 0.5$, $ET = 4$, then we get the following system:

$$\begin{cases} \left.\begin{array}{l} \frac{dx(t)}{dt} = \frac{1.5x(t)}{1+0.03y(t)} - 0.03x(t) - 0.02x^2(t) - 0.04x(t)y(t), \\ \frac{dy(t)}{dt} = 0.02x(t)y(t) + 0.1y(t) - 0.01y^2(t). \end{array}\right\} x \neq 4, \\ \left.\begin{array}{l} \Delta x(t) = -0.5x(t), \\ \Delta y(t) = -qy(t) + \tau. \end{array}\right\} x = 4. \end{cases} \tag{26}$$

On the one hand, if $\tau = 0$, let $q = 0.2$, and simple calculations show $\mu_2 = 0.86442 < 1$, then by Theorem 2, we get that system (5) has a stable boundary order-1 periodic solution $(x^T(t), 0)$ (see Figure 3). Let $q = 0.01$, by Theorem 2, there exists an unstable boundary order-1 periodic solution $(x^T(t), 0)$ for system (5) (see Figure 4, where $\mu_2 = 1.06972 > 1$).

On the other hand, if $\tau > 0$, by calculation, we have $y_{p_{ET}} = 21.177$. Let us choose $\tau = 3$; simple calculations show that $P_M(y_{p_{ET}}) = (1-q)y(ET, y_{p_{ET}}) + \tau = 17.2104 < y_{p_{ET}}$ holds. Then, by Theorem 4, the Poincaré map P_M only has a globally asymptotically stable fixed point y_f on $[0, y_{p_{ET}}]$ (see Figure 5a); as a result, system (5) has an order-1 periodic solution (see Figure 6a–c). If we let $\tau = 10$, then $P_M(y_{p_{ET}}) = (1-q)y(ET, y_{p_{ET}}) + \tau = 24.2104 > y_{p_{ET}}$ holds, and by Theorem 5, the Poincaré map P_M has a fixed point y_f on $(y_{p_{ET}}, +\infty)$(see Figure 5b). Therefore, system (5) has an order-1 periodic solution (see Figure 6d–f).

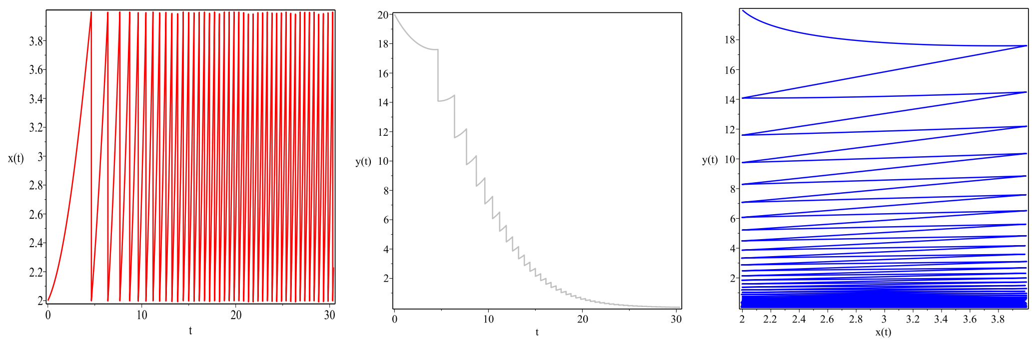

(**a**) (**b**) (**c**)

Figure 3. Existence and stability of the boundary order-1 periodic solution $(x^T(t), 0)$ for $\tau = 0$ in case I, with $\mu_2 < 1$, and where the initial value is $(2, 20)$. (**a**) Time series of x; (**b**) Time series of y; (**c**) Diagram of the relationship between x and y.

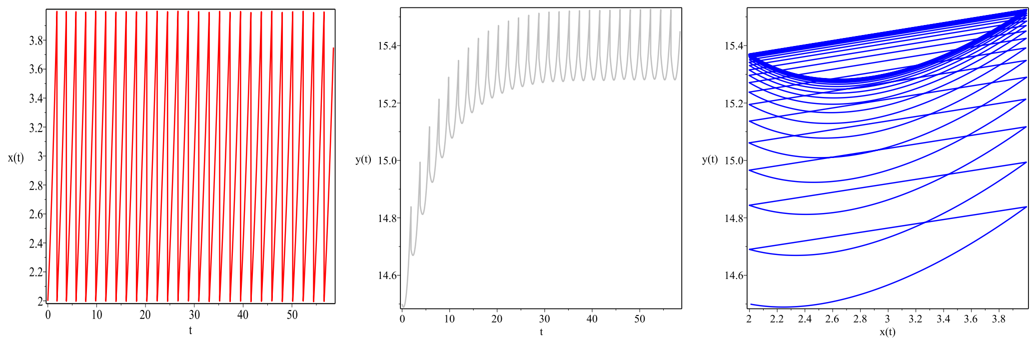

(**a**) (**b**) (**c**)

Figure 4. The instability of the boundary order-1 periodic solution $(x^T(t), 0)$ for $\tau = 0$ in case I, with $\mu_2 > 1$, and where the initial value is $(2, 14.5)$. (**a**) Time series of x; (**b**) Time series of y; (**c**) Diagram of the relationship between x and y.

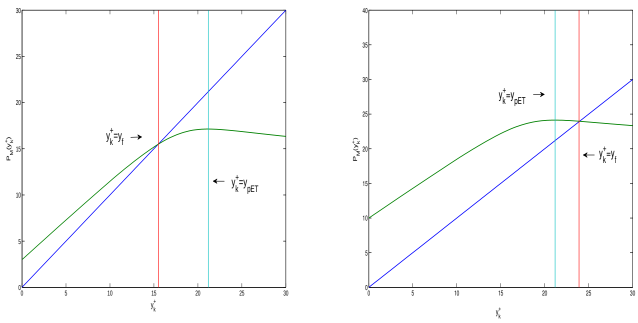

(**a**) (**b**)

Figure 5. The P_M of Case I, where $r_0 = 1.5, k = 0.03, a = 0.02, d = 0.03, b = 0.04, c = 0.5, m = 0.1,$ $h = 0.01, p = 0.5, q = 0.2$. (**a**) $\tau = 3$; (**b**) $\tau = 10$.

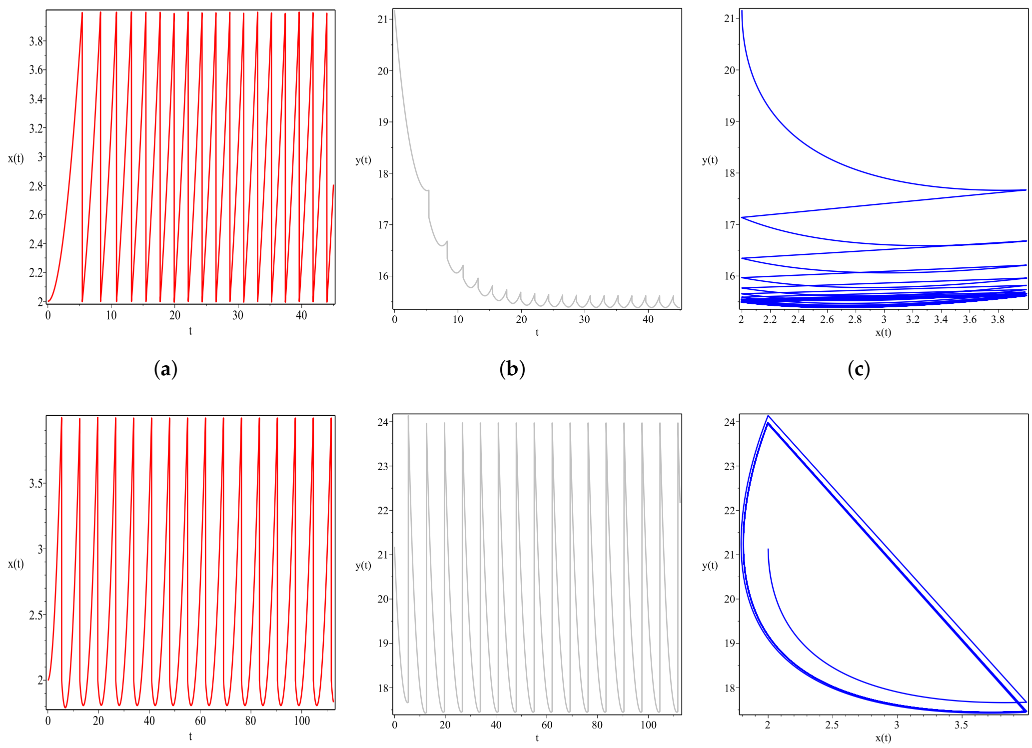

(**a**) (**b**) (**c**)

(**d**) (**e**) (**f**)

Figure 6. Existence and stability of the order-1 periodic solution for $\tau > 0$ in case I, where $r_0 = 1.5, k = 0.03, a = 0.02, d = 0.03, b = 0.04, c = 0.5, m = 0.1, h = 0.01, p = 0.5, q = 0.2$, and $\tau = 3$ for (**a**–**c**), $\tau = 10$ for (**d**–**f**), respectively. (**a**) Time series of x; (**b**) Time series of y; (**c**) Diagram of the relationship between x and y; (**d**) Time series of x; (**e**) Time series of y; (**f**) Diagram of the relationship between x and y.

For case IIa, let $ET = 6.4$ and $p = 0.85$, then we get the following system:

$$\begin{cases} \left.\begin{aligned} \frac{dx(t)}{dt} &= \frac{1.5x(t)}{1+0.03y(t)} - 0.03x(t) - 0.02x^2(t) - 0.04x(t)y(t), \\ \frac{dy(t)}{dt} &= 0.02x(t)y(t) + 0.1y(t) - 0.01y^2(t). \end{aligned}\right\} x \neq 6.4, \\ \left.\begin{aligned} \Delta x(t) &= -0.85x(t), \\ \Delta y(t) &= -qy(t) + \tau. \end{aligned}\right\} x = 6.4. \end{cases} \tag{27}$$

Obviously, it is easy to calculate that $Q(ET, y_{ET}) = (6.4, 19.682)$, $P_2(x_{p_2}, y_{p_2}) = (1.632, 21.312)$. For the case of $\tau = 0$, let $q = 0.3$, and we compute that $\mu_2 = 0.86557 < 1$; then, by Theorem 6, system (5) has a stable boundary periodic solution (see Figure 7). If we let $q = 0.1$, it is calculated that $\mu_2 = 1.11289 > 1$, and by Theorem 6, the boundary periodic solution for system (5) is unstable (see Figure 8).

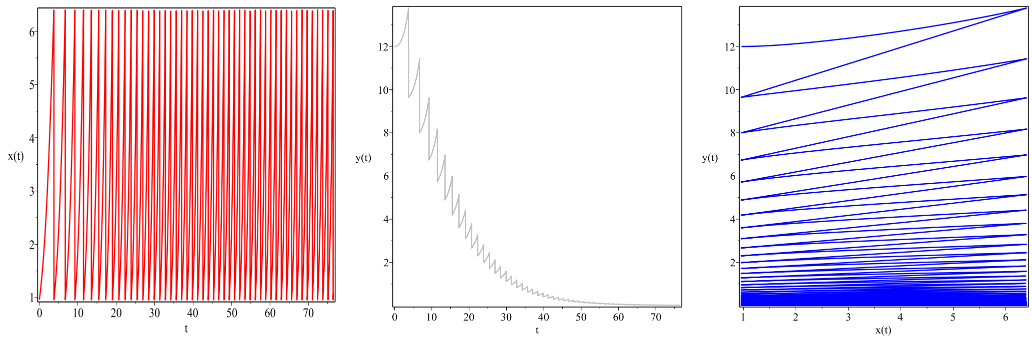

(**a**) (**b**) (**c**)

Figure 7. Existence and stability of the boundary order-1 periodic solution $(x^T(t), 0)$ for $\tau = 0$ in case IIa, with $\mu_2 < 1$, and where the initial value is $(0.96, 12)$. (**a**) Time series of x; (**b**) Time series of y; (**c**) Diagram of the relationship between x and y.

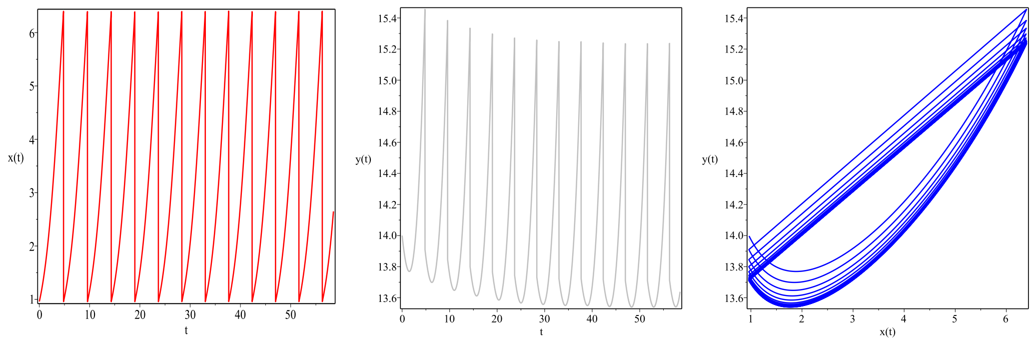

(**a**) (**b**) (**c**)

Figure 8. The instability of the boundary order-1 periodic solution $(x^T(t), 0)$ for $\tau = 0$ in case IIa, with $\mu_2 > 1$, and where the initial value is $(0.96, 14)$. (**a**) Time series of x; (**b**) Time series of y; (**c**) Diagram of the relationship between x and y.

For the case of $\tau > 0$, for example, let $\tau = 2$, then we get $P_M(y_{p_{ET}}) = 16.39405 < y_{p_{ET}} = B = 21.312$. By Theorem 8, the Poincaré map P_M has a globally asymptotically stable fixed point (see Figure 9a), and system (5) has a stable order-1 periodic solution (see Figure 10a–c)). If we let $\tau = 10$, then we get $P_M(y_{p_{ET}}) = 24.38607 > y_{p_{ET}}$. It can be obtained from Theorem 9 that the Poincaré map P_M has a globally asymptotically stable fixed point (see Figure 9b), and system (5) has an order-1 periodic solution (see Figure 10d–f).

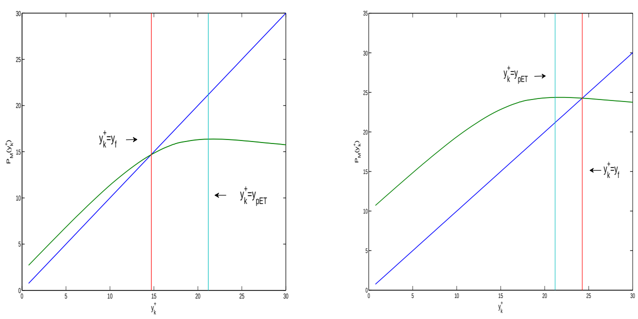

(**a**) (**b**)

Figure 9. The P_M for Case IIa, where $(1-q)ET < x_{p_2} < ET, p = 0.85, q = 0.2$. (**a**) $\tau = 2$; (**b**) $\tau = 10$.

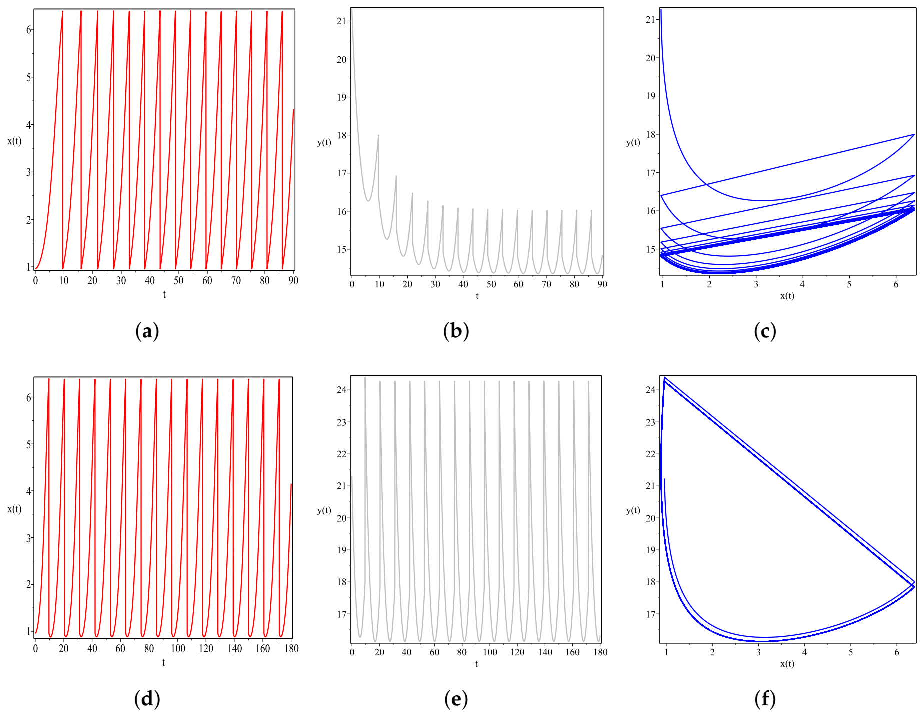

Figure 10. Existence and stability of the order-1 periodic solution for $\tau > 0$ in case IIa, where $r_0 = 1.5, k = 0.03, a = 0.02, d = 0.03, b = 0.04, c = 0.5, m = 0.1, h = 0.01, p = 0.85, q = 0.2$, and $\tau = 2$ for (**a**–**c**), $\tau = 10$ for (**d**–**f**), respectively. (**a**) Time series of x; (**b**) Time series of y; (**c**) Diagram of the relationship between x and y; (**d**) Time series of x; (**e**) Time series of y; (**f**) Diagram of the relationship between x and y.

In Case IIb, let $ET = 6.4$,$p = 0.5$, and $q = 0.2$; we then have the following system:

$$\begin{cases} \left.\begin{aligned} \frac{dx(t)}{dt} &= \frac{1.5x(t)}{1+0.03y(t)} - 0.03x(t) - 0.02x^2(t) - 0.04x(t)y(t), \\ \frac{dy(t)}{dt} &= 0.02x(t)y(t) + 0.1y(t) - 0.01y^2(t). \end{aligned}\right\} x \neq 6.4, \\ \left.\begin{aligned} \Delta x(t) &= -0.5x(t), \\ \Delta y(t) &= -0.2y(t) + \tau. \end{aligned}\right\} x = 6.4. \end{cases} \tag{28}$$

By direct calculation, we obtain $T_1((1-p)ET, y_{T_1}) = (3.2, 17.132)$, $T_2((1-p)ET, y_{T_2}) = (3.2, 30.510)$.

In this case, any trajectory beginning with $(x_0^+, y_0^+), y_0^+ \in I_s$ either experiences a finite number of pulses or an infinite number of pulses. Furthermore, we draw images of the Poincaré mapping under case IIb (see Figure 11). When $\tau = 1$, we get $P_M(y_{T_1}) = 16.41391 < y_{T_1} = 17.132$. From Figure 11a, we get that the fixed point y_f of system (5) is on $[0, 17.132]$, which confirms Theorem 10, and system (5) has a globally stable order-1 periodic solution (see Figure 12a–c).

From Figure 11b, when $\tau = 5 > 0$ and $17.132 < P_M(y_{T_1}) = P_M(17.132) = 20.41717 < 30.510$, P_M has no fixed point. Similarly, from Figure 12d–f, we know that there may be no periodic solution provided that $y_{T_1} < P_M(y_{T_1}) < y_{T_2}$. From Figure 11c, when $\tau = 25 > 0$ and $P_M(y_{T_1}) = P_M(17.132) = 40.41717 > 30.510$, the fixed point of P_M is on $(y_{T_2}, +\infty)$. Figure 12g–i verify that the order-1 periodic solution of system (4) is stable when $P_M(y_{T_1}) = 40.41717 > y_{T_2} = 30.510$.

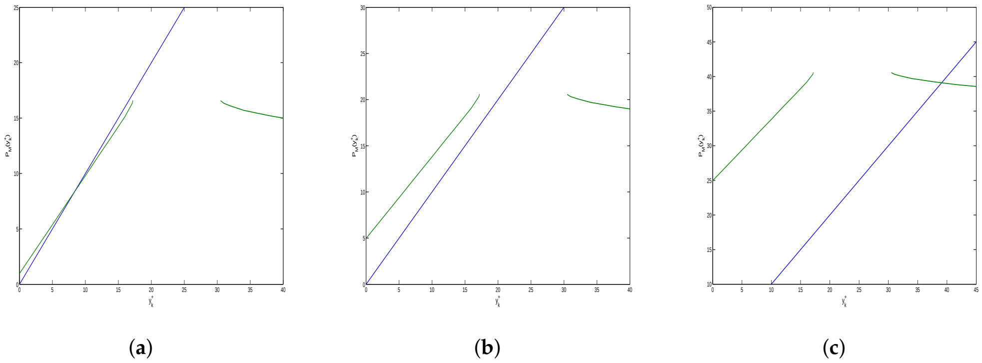

Figure 11. The P_M for Case IIb, where $x_{p_2} < (1-q)ET < ET, r_0 = 1.5, k = 0.03, a = 0.02, d = 0.03, b = 0.04, c = 0.5, m = 0.1, h = 0.01, p = 0.5, q = 0.2$. (**a**) $\tau = 1$; (**b**) $\tau = 5$; (**c**) $\tau = 25$.

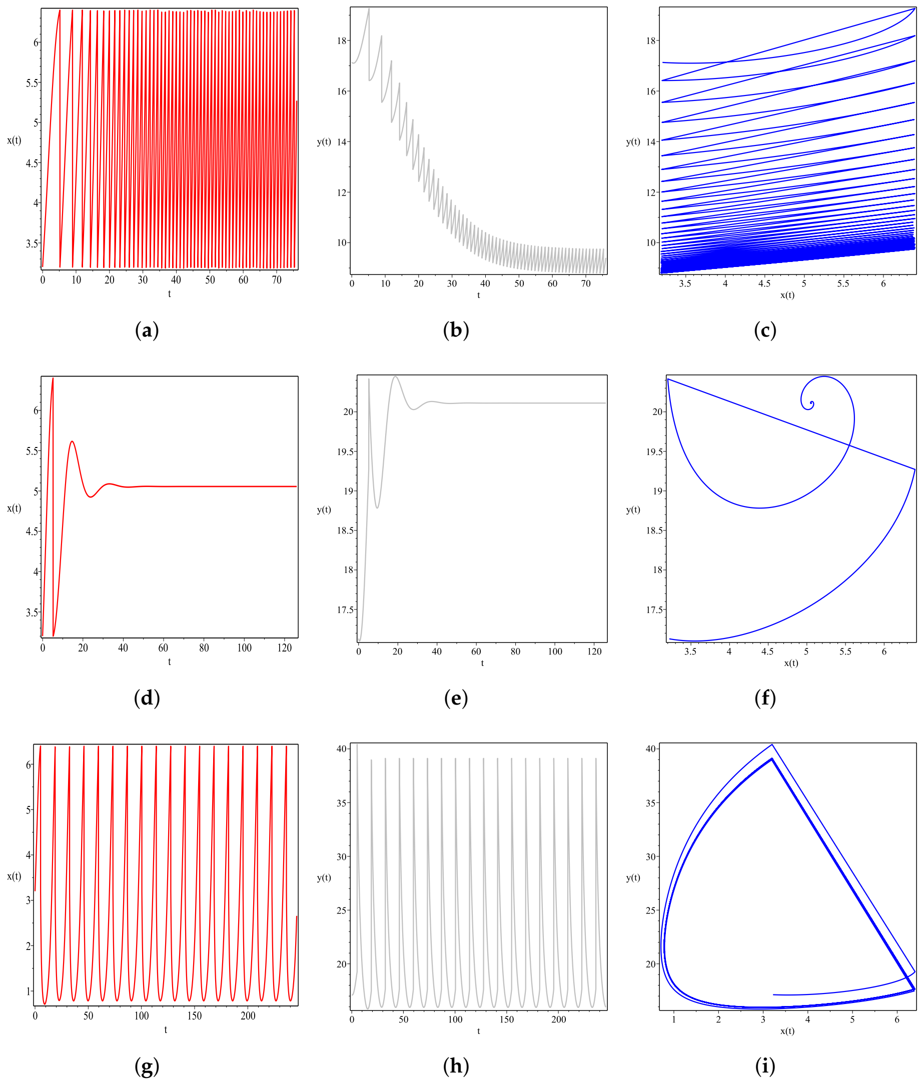

Figure 12. Existence and stability of the order-1 periodic solution for $\tau > 0$ in case IIb, where $r_0 = 1.5, k = 0.03, a = 0.02, d = 0.03, b = 0.04, c = 0.5, m = 0.1, h = 0.01, p = 0.5, q = 0.2$, and $\tau = 1$ for (**a**–**c**), $\tau = 5$ for (**d**–**f**), $\tau = 25$ for (**g**–**i**), respectively. (**a**) Time series of x; (**b**) Time series of y; (**c**) Diagram of the relationship between x and y; (**d**) Time series of x; (**e**) Time series of y; (**f**) Diagram of the relationship between x and y; (**g**) Time series of x; (**h**) Time series of y; (**i**) Diagram of the relationship between x and y.

Finally, we discuss the effect of the fear coefficient k on the dynamics of the system by numerical simulations. Since $R > 1$, we can then conclude that $k < \frac{1}{m}(\frac{r_0 h^2}{dh+mb} - 1)$. Let us take the following as parameters: $r_0 = 10, d = 0.3, a = 0.07, b = 0.1, c = 0.6, m = 0.1$, $h = 0.03$, $p = 0.3, q = 0.6, ET = 4, \tau = 10$; then we get $k < 4.4368$. Numerical simulations show that for $0 < k < 1.83$, system (5) has a stable order-1 periodic solution and for $k > 1.83$, the order-1 periodic solution disappears, and the solutions of system (5) tend to the positive equilibrium (see Figure 13).

Moreover, Figure 14 shows that when system (5) has a stable order-1 periodic solution, as the value of k increases, the oscillation of the prey population intensifies.

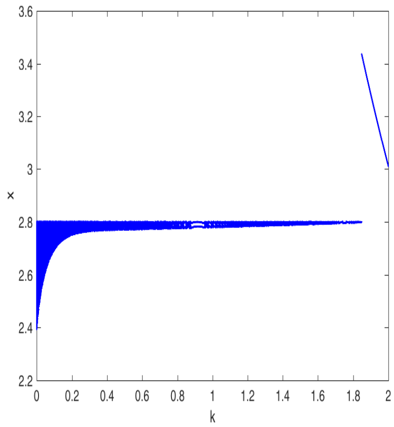

Figure 13. Branching diagram of parameter k, where $r_0 = 10, a = 0.07, d = 0.3, b = 0.1, c = 0.6$, $m = 0.1, h = 0.03, p = 0.3, q = 0.6, \tau = 10$.

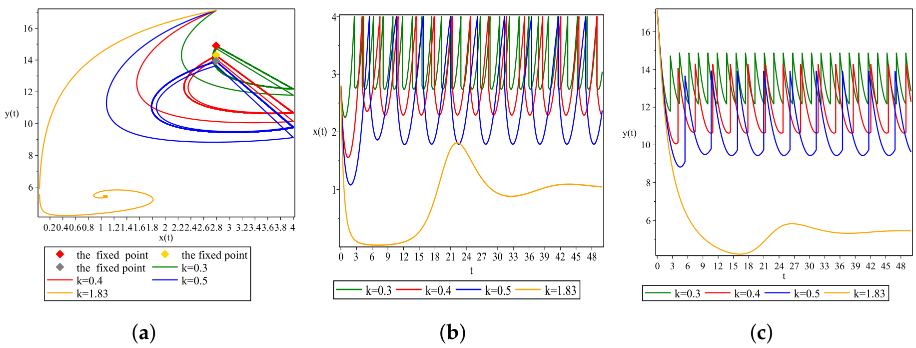

Figure 14. The influence of the fear effect on the system solution, where $r_0 = 10, a = 0.07, d = 0.3$, $b = 0.1$, $c = 0.6, m = 0.1, h = 0.03, p = 0.3, q = 0.6$, and $\tau = 10$. (**a**) Diagram of the relationship between x and y; (**b**) Time series of x; (**c**) Time series of y .

5. Conclusions

State-dependent impulse control has been applied to many aspects, and subsequently, it has been used in population ecology to study changes in biological populations in the last 20 years. Few papers have considered the problem of state feedback control with the fear effect on the prey or predator with additional food resources [61]. In reference [61], the author considered the state feedback control of a predator–prey model with the fear effect on prey; the model is as follows:

$$\begin{cases} \left.\begin{aligned} \frac{dx(t)}{dt} &= \frac{bx(t)}{1+ky(t)} - dx(t) - cx^2(t) - \frac{px(t)y(t)}{1+h_1x(t)}, \\ \frac{dy(t)}{dt} &= \frac{epx(t)y(t)}{1+(h_1+ph_2)x(t)} - my(t), \end{aligned}\right\} x \neq l, \\ \left.\begin{aligned} \Delta x(t) &= -q_1 x(t), \\ \Delta y(t) &= -q_2 y(t) + \tau. \end{aligned}\right\} x = l, \end{cases} \tag{29}$$

where x and y are the prey and the predator, respectively, b is the birth rate of the prey, k represents the fear effect of the predator on the prey, d represents the natural mortality rate of the prey, c is the mortality due to intraspecific competition of the prey, p is the predator for the predation rate of the prey, h_1 represents the time spent by the predator to capture the prey, h_2 represents the time spent on digesting the captured prey, e is the utilization rate of the predator by the predator, and m is the death rate of the predator. q_1 and q_2 are the catchability coefficient of prey and predator, respectively. l represents the optimal capture level of the prey. The author assumed that when the number of prey reaches the optimal capture level l, the prey and predator are harvested. In order to avoid long-term capture leading to the extinction of the predator population, an appropriate amount of τ predators is placed. For system (29), by establishing the corresponding Poincaré map, the authors proved the existence of the order-k periodic solutions for the system.

In system (29), the authors took into account the fear effect of predators and did not consider the additional food resources of predators, which created a model that ignores the effect of impulses simpler in structure than our model. More specifically, our model generates a new equilibrium point $E_2(0, \frac{m}{h})$, that although the prey eventually becomes extinct, because the predator has additional food resources, the predator may eventually exist. Therefore, the dynamics of our model are more complex and difficult to study for the problem of impulse feedback control, with both the fear effect on the prey and the additional food resources for the predator.

In this paper, we developed the application of state-dependent impulses by applying it to a predator–prey model, with the fear effect on the prey population and the additional food source for the predator population. In the model we built, we considered controlling the number of prey and predator populations based on the number of prey populations, hoping to achieve a certain balance of predators and prey. We constructed the Poincaré map of the state-dependent impulse system, and by analyzing the properties of Poincaré maps of pulse sets and phase sets at different positions, the dynamic properties of the system, including the existence, nonexistence, and stability of periodic solutions were investigated.

We found that the existence of the periodic solution for the system completely depends on the property of the Poincaré map. To verify the theoretical results we obtained, we gave some examples and numerical simulations for various cases. At the same time, numerical simulations also showed that the influence of the fear factor on the system is significant, that the increase of the fear factor makes the system periodic solution disappear, and that the predator and prey populations gradually stabilize to a level near the positive equilibrium.

Compared with the model without the state feedback control, the introduction of state feedback control makes the system dynamics more complicated. In [37], when $R < 1$, the system only had one stable equilibrium E_1; biologically, the pest population x would eventually tend to extinction, while the natural enemy population y would eventually tend to a constant $\frac{m}{h}$. Although the pests were eventually eradicated, this was a departure from the original purpose of integrated pest management. Note that when $R < 1$, the equilibrium E_2 is an unstable saddle point. Biologically, because the natural enemy population y has sufficient food sources, including pests and additional food resources, the population y will not become extinct in the end. However, for system (5), we controlled the pest population through an integrated pest management strategy, that is, by spraying pesticides and releasing natural enemies to control the pests. When $\tau = 0$, pests are controlled only by spraying pesticides. According to Theorems 1 and 2, when $\tau = 0$ and $\mu_2 < 1$, there is a stable boundary order-1 periodic solution for system (5). Biologically, the natural enemy population y may become extinct due to the overspraying of pesticides. When $R > 1$, system (4) has a stable equilibrium E_3 (stable node or focus); biologically, the pest population x and the natural enemy population y eventually tend to constants $x^*$and y^*, respectively. In order to achieve the maximum benefit of economic harvest without destroying the ecological balance, we adopted an integrated pest management strategy, that is, when the pest population x reached ET, the pests were controlled by spraying pesticides and releasing natural enemies. According to Theorems 4–9, there exists a globally asymptotically stable order-1 periodic solution for system (5). Biologically, the comprehensive implementation of pest control strategies makes the pest population x and natural enemy population y exhibit periodic oscillations.

Author Contributions: Writing—original draft preparation, Y.S.; writing—review and editing, T.Z. All authors worked together to produce the results. All authors have read and agreed to the published version of the manuscript.

Funding: This work was funded by the Shandong Provincial Natural Science Foundation, China under Grant Number ZR2019MA003 and by the Scientific Research Foundation of Shandong University of Science and Technology for Recruited Talents.

Institutional Review Board Statement: Not applicable.

Informed Consent Statement: Not applicable.

Data Availability Statement: Not applicable.

Conflicts of Interest: The authors declare that they have no competing interests.

References

1. Lotka, A.J. *Elements of Physical Biology*; Williams and Wilkins: Baltimore, MD, USA, 1926.
2. Volterra, V. Fluctuations in the abundance of a species considered mathematically. *Nature* **1926**, *118*, 558–560. [CrossRef]
3. So, J.W.; Freedman, H. Persistence and global stability in a predator-prey model consisting of three prey genotypes with fertility differences. *Bull. Math. Biol.* **1986**, *48*, 469–484. [CrossRef]
4. Holgate, P. A prey-predator model with switching effect. *J. Theor. Biol.* **1987**, *125*, 61–66.
5. Kareiva, P. Habitat fragmentation and the stability of predator–prey interactions. *Nature* **1987**, *326*, 388–390. [CrossRef]
6. Kuang, Y.; Smith, H.L. Global stability for infinite delay Lotka-Volterra type systems. *J. Differ. Equ.* **1993**, *103*, 221–246. [CrossRef]
7. Du, Y.; Lou, Y. S-shaped global bifurcation curve and Hopf bifurcation of positive solutions to a predator–prey model. *J. Differ. Equ.* **1998**, *144*, 390–440. [CrossRef]
8. Fussmann, G.F.; Ellner, S.P.; Shertzer, K.W.; Hairston, N.G., Jr. Crossing the Hopf bifurcation in a live predator-prey system. *Science* **2000**, *290*, 1358–1360. [CrossRef]
9. Sait, S.M.; Liu, W.C.; Thompson, D.J.; Godfray, H.C.J.; Begon, M. Invasion sequence affects predator–prey dynamics in a multi-species interaction. *Nature* **2000**, *405*, 448–450. [CrossRef]
10. Xiao, D.; Ruan, S. Global analysis in a predator-prey system with nonmonotonic functional response. *SIAM J. Appl. Math.* **2001**, *61*, 1445–1472. [CrossRef]
11. Xu, C.; Yuan, S.; Zhang, T. Average break-even concentration in a simple chemostat model with telegraph noise. *Nonlinear Anal. Hybrid Syst.* **2018**, *29*, 373–382. [CrossRef]
12. Liu, J.; Zhao, W. The dynamic analysis of a stochastic prey-predator model with markovian switching and different functional responses. *Math. Model. Appl.* **2018**, *7*, 12–21.
13. Liu, H.; Li, T.; Zhang, F. A prey-predator model with holling II functional response and the carrying capacity of predator depending on its prey. *J. Appl. Anal. Comput.* **2018**, *8*, 1464–1474.
14. Yu, X.; Yuan, S.; Zhang, T. Asymptotic properties of stochastic nutrient-plankton food chain models with nutrient recycling. *Nonlinear Anal. Hybrid Syst.* **2019**, *34*, 209–225. [CrossRef]
15. Jiang, H.; Tang, X. Hopf bifurcation in a diffusive predator-prey model with herd behavior and prey harvesting. *J. Appl. Anal. Comput.* **2019**, *9*, 671–690. [CrossRef]
16. Dondè, T. Uniform persistence in a prey–predator model with a diseased predator. *J. Math. Biol.* **2020**, *80*, 1077–1093. [CrossRef]
17. Cheng, H.; Hou, X. Study on the predator-prey model with Holling-Tanner functional response. *Math. Model. Appl.* **2021**, *10*, 32–43.
18. Xu, C.; Yuan, S.; Zhang, T. Competitive exclusion in a general multi-species chemostat model with stochastic perturbations. *Bull. Math. Biol.* **2021**, *83*, 1–17. [CrossRef]
19. Yao, W.; Li, X. Bifurcation difference induced by different discrete methods in a discrete predator-prey model. *J. Nonlinear Model. Anal.* **2022**, *4*, 69–79.
20. Lima, S. Nonlethal effects in the ecology of predator-prey interactions: What are the ecological effects of antipredator decision-making? *BioScience* **1998**, *48*, 25–34. [CrossRef]
21. Cresswell, W. Predation in bird populations. *J. Ornithol.* **2011**, *152*, 251–263. [CrossRef]
22. Creel, S.; Christianson, D. Relationships between direct predation and risk effects. *Trends Ecol. Evol.* **2008**, *23*, 194–201. [CrossRef]
23. Lima, S. Predators and the breeding bird: Behavioural and reproductive flexibility under the risk of predation. *Biol. Rev.* **2009**, *84*, 485–513. [CrossRef]
24. Preisser, E.L.; Bolnick, D.I. The many faces of fear: Comparing the pathways and impacts of nonconsumptive predator effects on prey populations. *PLoS ONE* **2008**, *3*, e2465. [CrossRef]

25. Pettorelli, N.; Coulson, T.; Durant, S.M.; Gaillard, J.M. Predation, individual variability and vertebrate population dynamics. *Oecologia* **2013**, *167*, 305–314. [CrossRef]
26. Peacor, S.D.; Peckarsky, B.L.; Trussell, G.C.; Vonesh, J.R. Costs of predator-induced phenotypic plasticity: A graphical model for predicting the contribution of nonconsumptive and consumptive effects of predators on prey. *Oecologia* **2013**, *171*, 1–10. [CrossRef]
27. Svennungsen, T.O.; Holen, Ø.H.; Leimar, O. Inducible defenses: Continuous reaction norms or threshold traits? *Am. Nat.* **2011**, *178*, 397–410. [CrossRef]
28. Feng, Z.; Chen, S.; Wei, J. Global dynamics of a diffusive leslie-gower predator-prey model with fear effect. *J. Nonlinear Model. Anal.* **2022**, *4*, 129–140.
29. Zanette, L.Y.; White, A.F.; Allen, M.C.; Clinchy, M. Perceived predation risk reduces the number of offspring songbirds produce per year. *Science* **2011**, *334*, 1398–1401. [CrossRef]
30. Hua, F.; Fletcher, R.J.; Sieving, K.E.; Dorazio, R.M. Too risky to settle: Avian community structure changes in response to perceived predation risk on adults and offspring. *Proc. R. Soc. B Biol. Sci.* **2013**, *280*, 20130762. [CrossRef]
31. Creel, S.; Christianson, D.; Liley, S.; Winnie, J.A. Predation risk affects reproductive physiology and demography of Elk. *Science* **2007**, *315*, 960. [CrossRef]
32. Sheriff, M.; Krebs, C.; Boonstra, R. The sensitive hare: Sublethal effects of predator stress on reproduction in snowshoe hares. *J. Anim. Ecol.* **2009**, *78*, 1249–1258. [CrossRef] [PubMed]
33. Wirsing, A.J.; Ripple, W.J. A comparison of shark and wolf research reveals similar behavioral responses by prey. *Front. Ecol. Environ.* **2011**, *9*, 335–341. [CrossRef]
34. Ninkovic, V.; Feng, Y.; Olsson, U.; Pettersson, J. Ladybird footprints induce aphid avoidance behavior. *Biol. Control* **2013**, *65*, 63–71. [CrossRef]
35. Khudr, M.S.; Buzhdygan, O.Y.; Petermann, J.S.; Wurst, S. Fear of predation alters clone-specific performance in phloem-feeding prey. *Sci. Rep.* **2017**, *7*, 7695. [CrossRef]
36. Wang, X.; Zanette, L.; Zou, X. Modelling the fear effect in predator-prey interactions. *J. Math. Biol.* **2016**, *73*, 1179–1204. [CrossRef]
37. Zhu, Z.; Wu, R.; Lai, L.; Yu, X. The influence of fear effect to the Lotka-Volterra predator-prey system with predator has other food resource. *Adv. Differ. Equ.* **2020**, *2020*, 237. [CrossRef]
38. Tang, S.; Cheke, R.A. State-dependent impulsive models of integrated pest management (IPM) strategies and their dynamic consequences. *J. Math. Biol.* **2005**, *50*, 257–292. [CrossRef]
39. Tang, S.; Xiao, Y.; Chen, L.; Cheke, R.A. Integrated pest management models and their dynamical behaviour. *Bull. Math. Biol.* **2005**, *67*, 115–135. [CrossRef]
40. Jiang, G.; Lu, Q. Impulsive state feedback control of a predator–prey model. *J. Comput. Appl. Math.* **2007**, *200*, 193–207. [CrossRef]
41. Tian, Y.; Sun, K.; Chen, L. Modelling and qualitative analysis of a predator-prey system with state-dependent impulsive effects. *Math. Comput. Simul.* **2011**, *82*, 318–331. [CrossRef]
42. Huang, M.; Liu, S.; Song, X.; Chen, L. Periodic solutions and homoclinic bifurcation of a predator–prey system with two types of harvesting. *Nonlinear Dyn.* **2013**, *73*, 815–826. [CrossRef]
43. Wei, C.; Chen, L. Heteroclinic bifurcations of a prey-predator fishery model with impulsive harvesting. *Int. J. Biomath.* **2013**, *06*, 1350031. [CrossRef]
44. Zhang, T.; Xu, T.; Wang, J.; Song, Y.; Jiang, Z. Geometrical analysis of a pest management model in food-limited environments with nonlinear impulsive state feedback control. *J. Appl. Anal. Comput.* **2019**, *9*, 2261–2277. [CrossRef]
45. Li, Z.; Wang, T.; Chen, L. Periodic solution of a chemostat model with Beddington-DeAnglis uptake function and impulsive state feedback control. *J. Theor. Biol.* **2009**, *261*, 23–32. [CrossRef]
46. Li, Z.; Chen, L. Periodic solution of a turbidostat model with impulsive state feedback control. *Nonlinear Dyn.* **2009**, *58*, 525–538. [CrossRef]
47. Sun, K.; Tian, Y.; Chen, L.; Kasperski, A. Nonlinear modelling of a synchronized chemostat with impulsive state feedback control. *Math. Comput. Model.* **2010**, *52*, 227–240. [CrossRef]
48. Tian, Y.; Kasperski, A.; Sun, K.; Chen, L. Theoretical approach to modelling and analysis of the bioprocess with product inhibition and impulse effect. *Biosystems* **2011**, *104*, 77–86. [CrossRef]
49. Li, Z.; Chen, L.; Liu, Z. Periodic solution of a chemostat model with variable yield and impulsive state feedback control. *Appl. Math. Model.* **2012**, *36*, 1255–1266. [CrossRef]
50. Guo, H.; Chen, L. Periodic solution of a chemostat model with Monod growth rate and impulsive state feedback control. *J. Theor. Biol.* **2009**, *260*, 502–509. [CrossRef]
51. Nie, L.; Teng, Z.; Hu, L. The dynamics of a chemostat model with state dependent impulsive effects. *Int. J. Bifurc. Chaos* **2011**, *21*, 1311–1322. [CrossRef]
52. Xiao, Y.; Miao, H.; Tang, S.; Wu, H. Modeling antiretroviral drug responses for HIV-1 infected patients using differential equation models. *Adv. Drug Deliv. Rev.* **2013**, *65*, 940–953. [CrossRef]
53. Tang, B.; Xiao, Y.; Tang, S.; Cheke, R.A. A feedback control model of comprehensive therapy for treating immunogenic tumours. *Int. J. Bifurc. Chaos* **2016**, *26*, 1650039. [CrossRef]
54. Tang, S.; Xiao, Y.; Wang, N.; Wu, H. Piecewise HIV virus dynamic model with CD4+ T cell count-guided therapy: I. *J. Theor. Biol.* **2012**, *308*, 123–134. [CrossRef]

55. Yang, Y.; Xiao, Y. Threshold dynamics for compartmental epidemic models with impulses. *Nonlinear Anal. Real World Appl.* **2012**, *13*, 224–234. [CrossRef]
56. Nie, L.F.; Teng, Z.D.; Guo, B.Z. A state dependent pulse control strategy for a SIRS epidemic system. *Bull. Math. Biol.* **2013**, *75*, 1697–1715. [CrossRef]
57. Zhao, T.; Xiao, Y. Non-smooth plant disease models with economic thresholds. *Math. Biosci.* **2013**, *241*, 34–48. [CrossRef]
58. Tang, S.; Liang, J.; Xiao, Y.; Cheke, R.A. Sliding bifurcations of Filippov two stage pest control models with economic thresholds. *SIAM J. Appl. Math.* **2012**, *72*, 1061–1080. [CrossRef]
59. Tang, S.; Tang, B.; Wang, A.; Xiao, Y. Holling II predator–prey impulsive semi-dynamic model with complex Poincaré map. *Nonlinear Dyn.* **2015**, *81*, 1575–1596. [CrossRef]
60. Xu, W.; Chen, L.; Chen, S.; Pang, G. An impulsive state feedback control model for releasing white-headed langurs in captive to the wild. *Commun. Nonlinear Sci. Numer. Simul.* **2016**, *34*, 199–209. [CrossRef]
61. Tian, Y.; Li, H. The study of a predator–prey model with fear effect based on state-dependent harvesting strategy. *Complexity* **2022**, *2022*, 9496599. [CrossRef]